

Subsurface Imaging of Integrated Circuits with Widefield and Confocal Microscopy Using Numerical Aperture Increasing Lens

F. Hakan Köklü¹, A. N. Vamivakas¹, J. I. Quesnel¹, S. B. Ippolito¹, B. B. Goldberg², and M. S. Ünlü¹
Boston University

¹Department of Electrical and Computer Engineering

²Department of Physics

Abstract— We report a lateral spatial resolution of $0.37\mu\text{m}$ with a custom infrared widefield microscope while imaging subsurface features in silicon integrated circuits from backside. In addition, $2.65\mu\text{m}$ apart polysilicon and metal layers can be differentiated.

I. INTRODUCTION

As succeeding generations of flip-chip integrated circuit (IC) fabrication technology has pushed minimum feature sizes to less than 100nm , the need to image subsurface features with deep submicron resolution has grown. This need is evidenced by the recent development of schemes to image such features with increasing resolution [1], [2], [3], [4]. Here, we report a lateral resolution of $0.37\mu\text{m}$ ($\lambda/3.24$) while imaging subsurface features of an IC from the backside using a custom infrared widefield microscope and a numerical aperture increasing lens (NAIL). This is far beyond the typical resolution of $1\mu\text{m}$ achieved by the state-of-the-art backside imaging techniques without NAIL. We can also resolve polysilicon and metal layers separated by $2.65\mu\text{m}$ longitudinally. We compare this to results obtained with a confocal microscope and a NAIL and discuss the relative advantages and disadvantages of the widefield microscope.

II. EXPERIMENT

Reflection mode infrared widefield and confocal microscopes were constructed to image subsurface features of a custom designed IC. The NAIL was an undoped silicon hemisphere with radius $R = 1.61\text{mm}$ which is convenient to do aplanatic imaging of a sample with a thickness of $470\mu\text{m}$ [5]. The IC that was employed for imaging consists of certain logic elements and the sufficient circuitry to support them with 4 metal and 2 poly layers. The structures used in this study are passive structures embedded into the first polysilicon layer of the IC. The design schematic of the imaged structures is shown in Fig. 1(a). The u values are $0.35, 0.6, 0.9, 1.2, 1.5$ and $2\mu\text{m}$ for the different passive structures. Front side image of these structures in Fig. 1(b) displays all six of them and the upper metal layers which makes these eligible to characterize the performance of NAIL imaging in an IC environment. The thickness of the IC was polished down to $470\mu\text{m}$ to

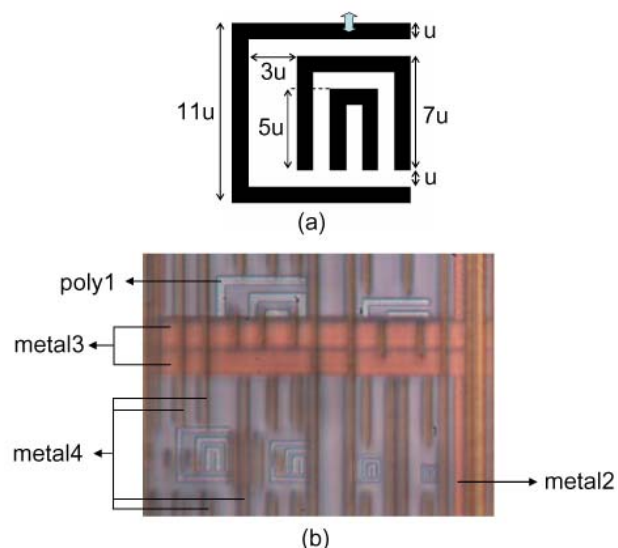


Fig. 1. (a) Drawing of the CNN logo. The sample has 6 CNN logos as scaled with $u = 0.35, 0.6, 0.9, 1.2, 1.5$ and $2\mu\text{m}$. The linecuts are taken at the top edge marked by the arrow. (b) Front side image of the sample with a commercial visible wavelength optical microscope. Notice the upper layers.

optimize the imaging with the NAIL. It was fabricated at Austriamicrosystems with $.35\mu\text{m}$ technology.

The confocal microscope constructed for this study consists of a diode laser for illumination ($\lambda=1.3\mu\text{m}$), a 2×2 fiber optic splitter, an optical fiber, an infinity corrected NIR 5X objective ($\text{NA}=0.14$) as the eyepiece, and an infinity corrected NIR 10X objective. Infrared radiation reflected from the sample is collected and collimated by the objective and then focused by the eyepiece onto the facet of the optical fiber. The signal transmitted through the 2×2 splitter is detected with a photodetector and recorded using LabVIEW software. The sample position is rastered using a piezoelectric translation stage.

The widefield microscope body consists of Thales Optem components: a near infrared (NIR) zoom module and a 2X tube lens. The illumination source is an LED array with a peak wavelength of 1200nm which is placed inside the Linos cage system. The objective used for the confocal microscope is also employed in this case for collection and the collimated signal

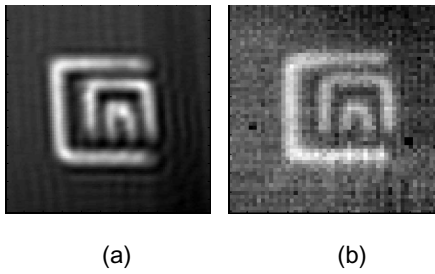


Fig. 2. (a) Confocal microscopy image of the CNN logo with $u = 0.35\mu\text{m}$. (b) Widefield microscopy image of the CNN logo with $u = 0.35\mu\text{m}$. The logo is resolved for both cases.

is reflected to the widefield scope by a sliding mirror. The collected radiation is imaged onto the CCD array (320x240 pixels) of a Sensors Unlimited InGaAs NIR camera. Camera images are recorded using a National Instruments (NI) image acquisition board together with NI Vision Assistant Software.

III. RESULTS

The images of the CNN logo (Fig. 1(a)) which has a u value of $0.35\mu\text{m}$ using confocal and widefield microscopes are shown in Fig. 2(a) and (b), respectively. As seen in the figure, the logo is resolvable for both confocal and widefield cases. The asymmetry of the image for the confocal case is attributed to the drift problems of the piezoelectric stage.

To characterize the performance of each microscope, we took a linecut at the top edge of the CNN logo with $2\mu\text{m}$ feature length. Error function is fit to the data for each case and line spread functions (LSF) are extracted as seen in Fig. 2. A resolution of $0.32\mu\text{m}$ ($\lambda/4$) and $0.37\mu\text{m}$ ($\lambda/3.24$) is calculated from the fits for the confocal and widefield imaging, respectively, according to Houston criterion. The data for the confocal case also exhibits the fringes as a direct consequence of coherent imaging [6]. This result is in agreement with the resolving capability shown in the images in Fig. 1. The main advantage of confocal microscopy over widefield microscopy is the depth sectioning ability. A longitudinal

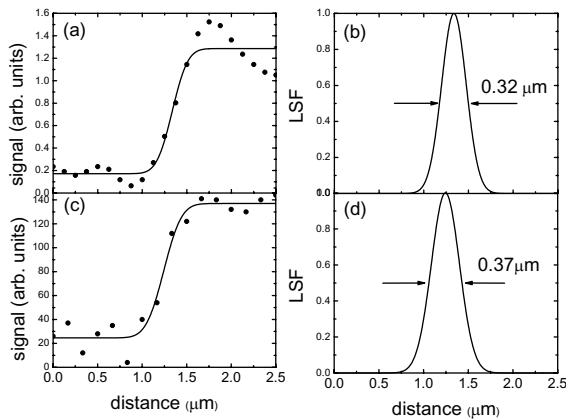


Fig. 3. (a) Data and the error function fit is seen for an edge using the confocal microscope. (b) Line spread function for (a). (c) Data and error function fit is seen for an edge using the widefield microscope. (d) Line spread function for (c).

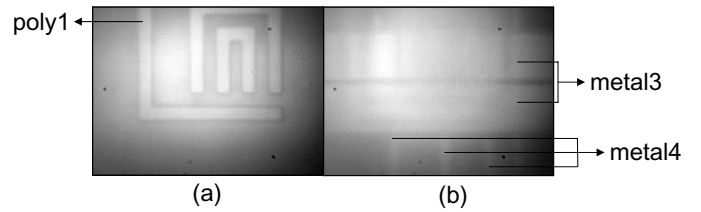


Fig. 4. Image of the same area while focusing different layers. (a) CNN logo with $u = 2\mu\text{m}$ is easily seen when focused at the poly1 layer. (b) The same area now focused at the metal3 layer. In (a) metal3 and metal4 are not seen and in (b) poly1 disappears. However, metal3 and metal4 cannot be imaged separately. According to the manufacturer, typical separation between poly1 and metal3 is $2.65\mu\text{m}$ whereas separation between metal3 and metal4 is $1\mu\text{m}$.

resolution of better than $1.7\mu\text{m}$ was reported previously for confocal microscopy with a NAIL [7]. We tried to characterize the performance of the widefield microscope in terms of layer discrimination. In order to do that we imaged the biggest CNN logo which has a $u = 2\mu\text{m}$. As seen in Fig. 1(b), a thick wire of metal3 is passing above it which makes it very difficult to image from the front side. When we image the same area from the backside with the help of the NAIL, we could image both layers separately as depicted in Fig. 4. The separation between poly1 and metal3 varies from $1.65\mu\text{m}$ to $3.65\mu\text{m}$ with a typical separation of $2.65\mu\text{m}$. However, as seen in Fig 4 (b), metal3 and metal4 layers having a typical separation of $1\mu\text{m}$ cannot be imaged separately.

IV. CONCLUSIONS

Continuous increase of technical specifications for IC fabrication require robust failure analysis capabilities which make it necessary to realize high resolution subsurface imaging tools. We have demonstrated lateral spatial resolutions of $0.37\mu\text{m}$ ($\lambda/3.24$) and $0.32\mu\text{m}$ ($\lambda/4$) while imaging multiple layered silicon ICs using widefield and confocal microscopy, respectively, with a numerical aperture increasing lens. In addition, separate imaging of structures in poly1 layer and metal3 layer with a total interlayer thickness of $2.65\mu\text{m}$ has been demonstrated. Widefield imaging seems to be promising for failure analysis when this submicron resolution and layer discrimination ability is supported with the enhanced rate of image acquisition and simpler optical systems.

REFERENCES

- [1] S. B. Ippolito, B. B. Goldberg, and M. S. Ünlü, "High spatial resolution subsurface microscopy," *App. Phys. Lett.*, vol. 78, p. 4071, June 2001.
- [2] J. Christofferson and A. Shakouri, "Thermoreflectance based thermal microscope," *Rev. of Sci. Inst.*, vol. 76, p. 024903, February 2005.
- [3] C. Saloma, A. Tarun, M. Bailon, and M. Soriano, "Rapid subsurface detection of nanoscale defects in live microprocessors by functional infrared emission spectral microscopy," *App. Opt.*, vol. 44, p. 7302, December 2005.
- [4] E. Ramsay, K. A. Serrels, M. J. Thomson, A. J. Waddie, M. R. Taghizadeh, R. J. Warburton, and D. T. Reid, "Three-dimensional nanoscale subsurface optical imaging of silicon circuits," *App. Phys. Lett.*, vol. 90, p. 131101, March 2007.
- [5] S. B. Ippolito, B. B. Goldberg, and M. S. Ünlü, "Theoretical analysis of numerical aperture increasing lens microscopy," *J. of App. Phys.*, vol. 97, p. 053105, 2005.
- [6] T. Wilson and C. Sheppard, *Theory and Practice of Scanning Optical Microscopy*. Academic Press, 1984.
- [7] S. Ippolito, *High Spatial Resolution Subsurface Microscopy*. PhD thesis, Boston University, 2004.